QUANTITATIVE PHASE IMAGING FOR BLOOD CYTOMETRY

BY

MUSTAFA AIZED HASAN MIR

THESIS

Submitted in partial fulfillment of the requirements
for the degree of Master of Science in Electrical and Computer Engineering
in the Graduate College of the
University of Illinois at Urbana-Champaign, 2010

Urbana, Illinois

Adviser:

Assistant Professor Gabriel Popescu

ABSTRACT

Blood smear analysis has remained a crucial diagnostic tool for pathologists despite the advent of automatic analyzers such as flow cytometers and impedance counters. Though these current methods have proven to be indispensable tools for physicians and researchers alike, they provide limited information on the detailed morphology of individual cells and merely alert the operator to manually examine a blood smear by raising flags when abnormalities are detected. Here I demonstrate an automatic *interferometry based* smear analysis technique known as Diffraction Phase Cytometry (DPC), which is capable of providing the same information on red blood cells as is provided by current clinical analyzers, while rendering additional, currently unavailable parameters on the 2D and 3D morphology of individual red blood cells (RBCs). To validate the utility of the technique in a clinical setting, I present a comparison between tests generated from 32 patients by a state-of-the-art clinical impedance counter and DPC.

The majority of work presented in this thesis is drawn from two publications: M. Mir et al., Journal of Biomedical Optics, vol. 15 (2), 2010, and M. Mir et al. Optics Express, vol. 17, 2009.

ACKNOWLEDGMENTS

I would like to thank my parents for the encouragement and support necessary to get this far. Also I'd like to thank my adviser, collaborators and colleagues for all their help with this project. This research was supported in part by the Grainger Foundation and the National Science Foundation (CAREER 08-46660).

CONTENTS

1 INTRODUCTION 1
2 DIFFRACTION PHASE MICROSCOPY 4
3 BLOOD ON A CD-ROM 7
4 CLINICAL APPLICATIONS 18
5 DISCUSSION 28
REFERENCES 30

1. INTRODUCTION

When Robert Hooke and Anton van Leeuwenhoek first observed cells, microorganisms and other microscopic structures using the earliest bright-field light microscopes in the 17th century, the fields of cell biology and optical microscopy were simultaneously born. However the major challenge with observing thin transparent samples, such as most biological tissue, and cells, is that they have little effect on the amplitude of an optical field propagating through them, and thus there is almost no contrast measurable by eyes or detectors. However, due to the difference in the refractive index between the cells and their surrounding environment, the speed of light inside the cells is slower. This means the phase front of the optical field passing through the cells is modulated compared to the background; thus, such objects are appropriately called phase objects. For almost 400 years, this challenge was addressed through the use of extrinsic contrast agents or stains that absorb light, which meant that cells often needed to be fixed and could not be observed in their natural state.

The breakthrough came in 1934, when the Dutch scientist Frits Zernike revolutionized microscopy through the invention of phase contrast (PC) [1]. PC enhances contrast in phase objects by optically mapping small variations in phase, to a measurable change in amplitude. Since then, optical phase shift has been used as a powerful endogenous contrast agent. The major physical insight that led to this discovery can be attributed to Ernst Abbe for his description of a microscope image, best summarized in his own words: "The microscope image is the interference effect of a diffraction phenomenon" [2]. This lead to the idea of spatially decomposing an optical field into its spatial average (un-scattered, U_0) and spatially varying (scattered, $U_1(x,y)$) components. This means that the image field $U_i(x,y)$ may be written as

$$U_i(x,y) = U_0 + [U_i(x,y) - U_0] = U_0 + U_1(x,y) \tag{1.1}$$

where we can write the average field U_0 as

$$U_0 = \frac{1}{A}\iint U_i(x,y)dxdy = \langle U_i(x,y)\rangle_{x,y} \tag{1.2}$$

where A is the area of the image. It is important to note that this is only true when the coherence area of the field is larger than the field of view. The resulting intensity that is recorded by a CCD can thus be written as an interferogram

$$I(x,y) = |U_i(x,y)|^2 = |U_0|^2 + |U_i(x,y)|^2 + 2|U_0||U_i(x,y)|\cdot\cos[\Delta\phi(x,y)] \tag{1.3}$$

where $\Delta\phi(x,y)$ is the phase difference between the two fields. For optically thin objects, such as biological cells and tissue, there is essentially no intensity modulation and $\Delta\phi(x,y)$ exhibits small variations, thus the cosine term varies slowly. However if an additional phase shift of $\pi/2$ is added to the phase, the cosine is replaced with a sine, which varies quickly for small values of $\Delta\phi(x,y)$. Taking advantage of this idea and the Fourier transform (FT) property of lenses, Zernike was able to optically shift the phase of these components by $\pi/2$, which made them interfere with greater contrast. He was awarded the 1953 Nobel Prize in Physics for his contribution.

Despite the power of PC, the relationship between irradiance and phase in PC is non-linear, and thus the optical path length difference between the cell and its environment cannot be quantified. Thus, several different methods have been developed to measure the complex optical field in microscopy, including holographic microscopy and a vast array of clever interferometric techniques lumped together in the field dubbed quantiative phase imaging (QPI). QPI techniques, as the name suggests, measure the phase shift induced by a specimen. This is accomplished by mixing the image field (U_i) with a reference field (U_r) so that the intensity recorded by a CCD placed at the image plane contains information about the phase,

$$I(x,y) = |U_i(x,y)|^2 + |U_r|^2 \\ +2|U_i(x,y)||U_r|\cos\left[\langle w\rangle(t-t_r) - (\langle \mathbf{k}\rangle - \mathbf{k_r})\mathbf{r} + \phi(x,y)\right] \tag{1.4}$$

where <ω> is the mean frequency and <**k**> is the mean wave vector. By modifying the time delay, τ_r, or modifying the direction of propagation, $\mathbf{k}_r$, of the reference field, the quantity of interest, □(x,y), may be extracted. Modulating the time delay is known as phase-shifting interferometry and tilting the reference beam is known as off-axis interferometry. The major issue with traditional interferometry setups is that the reference and sample arms are separated spatially and combined with a beam splitter at the CCD plane. This means that two fields experience noise that is uncorrelated and cannot be subtracted. Traditional ways to get around this include using passive stabilization techniques such as a damped optical table or active techniques that require some sort of feedback mechanism. A more elegant way to resolve this issue is through the use of common path techniques in which the reference and sample field are practically overlaid.

In this thesis we will discuss the principle behind Diffraction Phase Microscopy (DPM) [3], an off-axis, common-path, full-field technique. We will discuss the application of this technique for blood cytometry. To prove the utility of the method, a clinical trial was conducted, which marks the first use of a QPI technique in a clinical setting.

2. DIFFRACTION PHASE MICROSCOPY

2.1 Common Path Interferometry

Diffraction phase microscopy (DPM) is a full-field common path interferometery technique introduced by Popescu et. al in 2006 [3]. Figure 2.1 below shows a DPM setup. The illumination source may be selected depending on the application at hand, and any source is sufficient as long as it is spatially coherent. Since DPM is usually implemented as an add-on to an inverted microscope, the only additional components that are necessary are a relay lens, a diffraction grating, and a 4-f spatial filtering setup. The image plane from the microscope is projected onto the diffraction grating via the relay lens. This generates several diffraction orders in the Fourier plane, which is projected onto the spatial filter via lens L1. Each of the diffraction orders contains complete information of the field at the sample plane. The spatial filter is placed in the Fourier plane such that only the DC component of the 0th order spot is allowed to pass, which serves as the reference beam, and the entire frequency range of the 1st order beam is passed, which serves as the sample beam. Lens L2 is the inverse Fourier lens in the 4-f system and projects the interferogram onto a CCD.

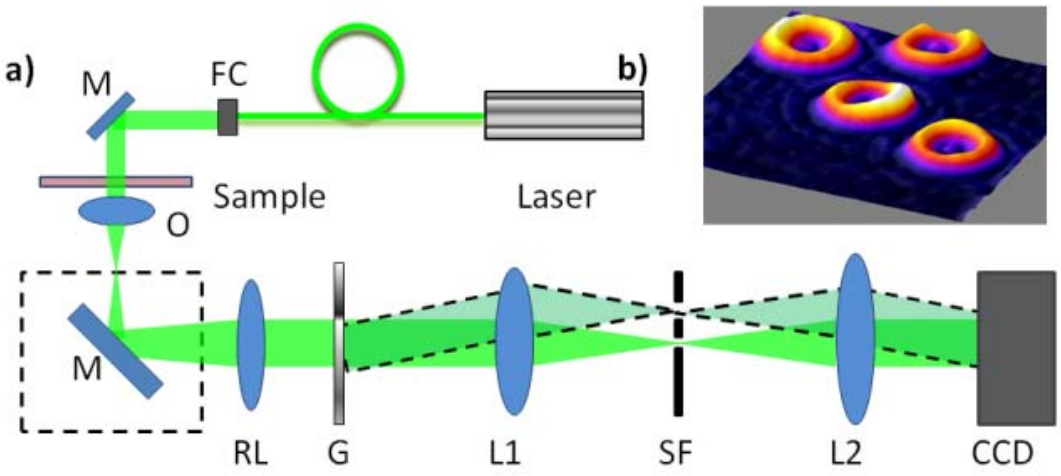

Fig. 2.1 DPM schematic: a) FC, fiber collimator; M, mirror; S, sample; O, objective lens; TL, tube lens; G, grating; SF, spatial filter; L1 and L2, lenses. b) Close-up of a DPC image of 4 RBCs.

2.2 Phase Reconstruction

The CCD recording may be written as

$$I(x,y) = \left|U_i(x,y)\right|^2 + \left|U_r\right|^2 + 2\left|U_i(x,y)\right|\left|U_r\right|\cos\left[qx + \phi(x,y)\right] \tag{2.1}$$

where q is the spatial frequency shift from the diffraction grating. The interferogram is then spatially high-pass filtered to isolate the sinusoidal cross term. For phase objects, $U_1(x,y)$ is expected to have weak spatial dependence and thus the isolated term can be interpreted as the real part of a spatial complex analytic signal. The corresponding imaginary part can then be obtained via a Hilbert transform:

$$\sin\left[qx + \phi(x,y)\right] = P\int \frac{\cos\left[qx^2 + \phi(x',y)\right]}{x - x'} \tag{2.2}$$

where P is the principle value integral. The phase may then be recovered as

$$\phi(x,y) + qx = \arg\left[\cos\left(qx + \phi\right), \sin\left(qx + \phi\right)\right] \tag{2.3}$$

The diffraction limited resolution of the system can be preserved through proper selection of the spatial modulation, q. As with any other signal, this must meet the requirements of the Nyquist theorem, that it is twice the highest resolvable frequency. Since this value q is known from the period of the diffraction grating, it may simply be subtracted to retrieve $\varphi(x,y)$. However since qx can be much higher than 2π, $\varphi(x,y)+qx$, can be highly wrapped. An unwrapping algorithm is thus applied prior to subtracting qx. Such algorithms search for 2π jumps in the phase and correct them. In this manner the phase can be recovered from a single CCD recording.

2.3 Summary

In the next chapters we will discuss how the DPM idea may be implemented in an even more compact form using a commercial CD-ROM and spatial light modulator (SLM), and how physiologically relevant morphologial parameters may be extracted from the measured phase

maps. I dubbed this technique of extracting single cell parameters from DPM measurements as Diffraction Phase Cytometry (DPC).

3. BLOOD ON A CD-ROM

3.1 Why Blood Screening?

Existing clinical technologies used to characterize patient blood such as impedance counters and flow cytometers, though very effective in terms of throughput, offer limited information, are expensive, bulky, costly to maintain, and often require careful calibration. Though there have been reports of using high throughput cytometers to characterize red cell morphology [4], this approach is limited as it only provides a general description of shape (eg. ellipsoid vs. spherical) and is unable to provide the resolution required for aiding in differential diagnosis. Automated counters are thus designed to produce accurate measurements of normal blood and to alert the technician with "flags" when numerical abnormalities exist so that a smear may then be prepared and examined [5]. Even though automated blood analyzers have reduced the number of samples that require smears to 15%, the examination of a smear is still an indispensable tool in providing differential diagnosis (commonly for anemias and thrombocytopenia), recommending further tests, speedy diagnosis of certain infections and the identification of leukemia and lymphoma [6]. Despite the ability of the automated instruments to measure volume and hemoglobin concentrations, they are unable to accurately measure morphologic abnormalities and variations in shape, at the single cell level, and thus a pathologist is required to manually examine a smear. Other modern methods that can be used for accurately assessing red cell morphology, such as confocal microscopy, suffer from complicated procedures and the need for using specialized exogenous contrast agents.

The use of the optical phase shift through a sample as an endogenous contrast agent has served as a powerful technique in microscopy since the advent of techniques such as phase contrast (PC) and differential interference contrast (DIC) microscopy [7]. Even though these

modalities greatly enhance the ability to observe details within transparent objects such as living cells, it was not until the development of quantitative phase imaging (QPI) techniques that the phase shift through a sample was able to provide quantitative information. Furthermore, with the development of common path interferometry and methods such as diffraction phase microscopy [3], we can obtain quantitative phase images that are sensitive to sub-nanometer changes in optical path lengths over broad temporal scales.

In this chapter, we present diffraction phase cytometry (DPC) as a single shot, full-field, high throughput QPI technique that is capable of taking direct measurements of cell morphology by measuring the optical path length difference between the cell and its surrounding medium. We demonstrate the principle of implementing blood cytometry in a "lab-on-a-chip" instrument which will be inexpensive and highly portable. With further refinements, such an instrument will make QPI technology available to any clinic with a modern computer and allow for a detailed analysis that is currently not possible without access to expensive instruments such as flow cytometers.

3.2 Experimental Setup

The DPC setup is illustrated in Figure 3.1. A frequency-doubled Nd:YAG laser (λ=532 nm) was used as the illumination source for an inverted microscope (MEIJI Techno TC5200) equipped with a 20X, 0.4 NA objective. With the tube lens of the microscope removed, the Fourier transform of the microscope image is projected on the SLM plane, which is used as a spatial filter as shown in Figure 3.1. The SLM used is a liquid crystal display (LCD) sandwiched between a polarizer and an analyzer and was extracted from a commercial digital LCD projector (EPSON). The SLM is controlled via the green channel of a standard RGB monitor signal [8]. Each pixel on the SLM is 13.7 μm^2 with a total size of 800 x 600 pixels, and has a dynamic

range of 256 grey values. The lens L1 acts as the inverse transformer and projects the magnified microscope image plane onto its front focal plane, where it is recorded by the CCD. The CCD is operated in 2x2 binning mode and the image resolution is 1024 x 768 pixels where each pixel is ~ 5x5 μm^2; the field of view of the image is 180 x 135 μm^2, and the total magnification of the system is ~ 30X.

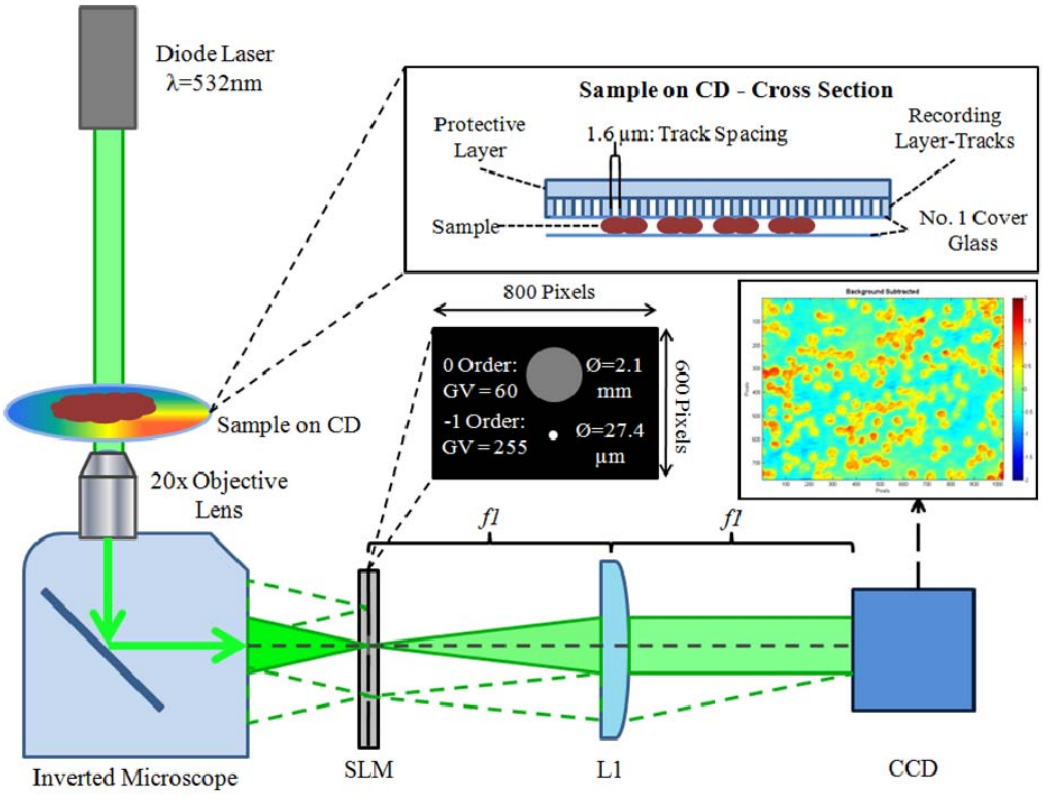

Fig. 3.1 DPC setup. SLM, spatial light modulator; L1, lens; focal length, *f1*=300 mm; GV, grey value of pixels; Ø, diameter of pinholes.

A commercial blank compact disk with its label peeled off is placed at the object plane of the microscope. The tracks on the CD serve as a 1.6 μm pitch transmission diffraction grating (see Figure 3.1 inset), which generates several diffraction orders at the SLM plane, each containing full spatial information about the sample placed on the CD. The SLM is then used to spatially low-pass filter the 1st order beam by passing it through a pinhole mask with a diameter of Ø=27.4 μm so that it is proportional to the spatial average of the image field and is thus

appropriate for use as the reference field in a common-path Mach-Zender interferometer. The entire frequency content of the 0^{th} order beam is allowed to pass and thus serves as the object field; all the other orders are blocked entirely. Since the 0^{th} order beam has a significantly higher intensity than the 1^{st} order, we adjusted the SLM voltage such that it selectively attenuates and levels the intensities of the two beams, for maximum fringe contrast. The ability to adjust the contrast between the two interfering fields represents a significant improvement with respect to using a conventional pinhole. This setup provides spatial sampling of the image at 16 CCD pixels/period. Quantitative phase information is then retrieved from the interferograms as described in Chapter 2.

In order to correct for aberrations and background noise, we estimated and subtracted the background, a constant characteristic of the instrument, using a least squares regression fit to a polynomial of the form: $B(x,y)=b_0x^2+b_1y^2+b_2xy+b_3x+b_4y+b_5$ (via a MATLAB routine developed in-house). The subtraction is used to remove the low-frequency non-uniformities in the image (due to residual aberrations, etc). This background does not vary significantly over the size of the cell and, thus, does not affect the volume measurement. However, having a flat background provides a common reference for estimating the cell volumes automatically for a large number of cells.

3.3 Red Blood Cell Morphology

To demonstrate the ability of the DPC system to perform detailed cytometry type measurements, we imaged mature erythrocytes in peripheral blood smear samples from a healthy adult male and retrieved medically relevant geometric parameters such as volume (V), surface area (SA), sphericity index, and minimum cylindrical diameter (MCD) as described by Canham and Burton [9]. Erythrocytes or red blood cells (RBCs) are the dominant cell type in whole blood and are

thus a good candidate for testing our DPC system. RBCs are relatively simple in structure, with a homogeneous interior, and are also an excellent indicator of the physiological condition of a patient [5]. The blood smears were prepared by simply sandwiching a droplet of whole blood, obtained by finger prick, between two No. 1 cover slips. The sample is then placed between the CD and the objective as shown in Figure 3.1. Imaging is done immediately after preparation of the sample to minimize effects from drying. From the reconstructed quantitative phase maps we can simply relate the measured phase shift $\Delta\varphi(x,y)$ to sample height by

$$h(x, y) = 2\pi\lambda\Delta\phi(x, y) / \Delta n \tag{3.1}$$

where $\Delta n = n_{plasma} - n_{RBC}$ is the difference in the indices of refraction of the erythrocytes and the plasma, $n_{plasma} = 1.3515$ and $n_{RBC} = 1.3871$ [10, 11]. For comparison purposes we also measured 35, 4.5 μm diameter polystyrene microspheres (Polybead) suspended in immersion oil (Zeiss). The standard deviation for the microspheres is reported by the manufacturer as $\sigma = 0.236$ μm and the reported indices of refractions are $n_{microspheres} = 1.59$ and $n_{oil} = 1.518$ for the microspheres and oil respectively. The measured height distributions for both samples are shown in Figure 3.2. From the microsphere measurements (4.44 ±0.243 μm) shown below, it is clear that the DPC system correctly retrieves the height of a sample if the refractive indices are known.

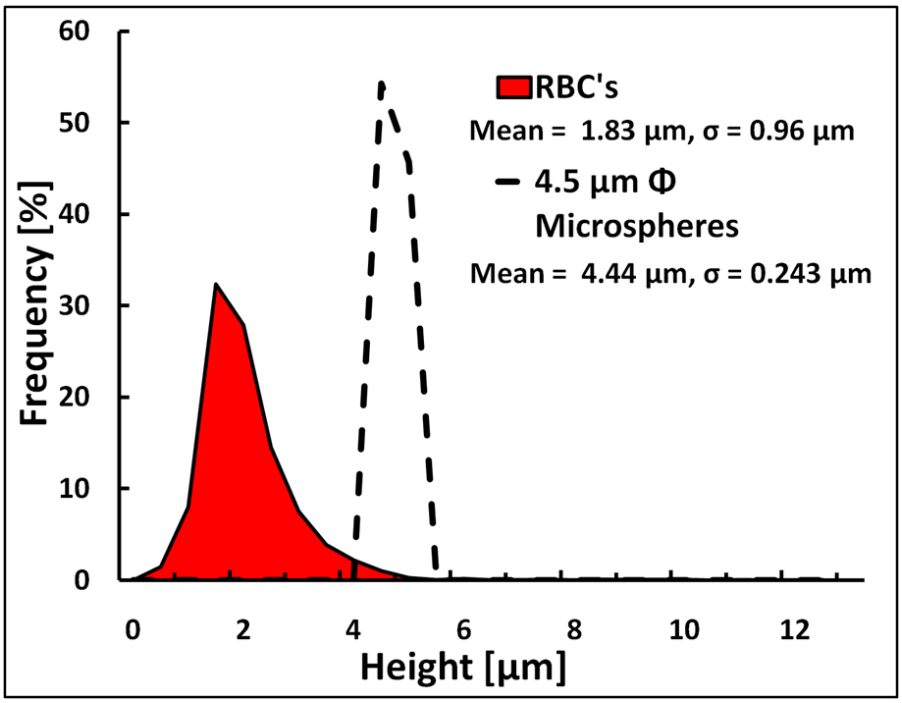

Fig. 3.2 Unbiased height frequency distribution for RBCs and a control sample of 4.5 µm polystyrene microspheres.

To aid the analysis, image processing software was developed in MATLAB to automatically detect and analyze the erythrocytes. In order to retrieve relevant information from the phase maps, the program implements a typical particle detection scheme utilizing a watershed algorithm, a distance transform and an H-minima transform [12] to obtain a list of coordinates occupied by individual erythrocytes. Considering the broad nature of the height distribution, to differentiate between individual cells, cell aggregates, debris and other cell types present in the samples, only regions with mean heights between 1.25 and 1.8 µm were considered. These values were chosen based on the observed mean values of erythrocytes with the refractive index values reported in the literature. For future studies with whole blood samples, this restriction can be refined to also include populations of leukocytes and platelets. The methods used to calculate the three-dimensional parameters such as volumes, surface area, sphericity and the minimum cylindrical diameter are described below, whereas parameters such as diameter, projected area,

perimeter and eccentricity were retrieved directly using region property descriptors available in MATLAB.

Volume: The volumes of individual erythrocytes were calculated by integrating the height map over the area of the cell. The mean cell volume reported here (69 +/-23 fL) is smaller than the average values in the literature (80-90 fL), which might be due to small refractive index deviation from the assumed value [10]. The shape of the volume distribution and its relative modifications with respect to normal conditions have been widely used for clinical diagnosis and shown to be a reliable indicator of various physiological conditions ranging from anemia and vitamin B12 deficiency to nicotine and alcohol addiction[5].

Surface Area: The surface areas of individual erythrocytes were measured by calculating a three-dimensional triangular mesh that conforms to the surface of the erythrocytes and then calculating the area of this mesh. Since our measurement is only sensitive to changes in optical path length, the area of the cell membrane was approximated as $SA = 2 * SAC + P * h_{\min}$, where SAC is the mesh surface area, P is the perimeter of the cell and h_{min} is the minimum optical path difference in the region occupied by the cell. To our knowledge, this is the first measurement of erythrocyte surface areas using a quantitative phase technique.

Sphericity: The sphericity of an erythrocyte is a dimensionless parameter first described by Canham and Burton [9] and is a measure of how spherical a cell is, with values between 0 and 1, for a sphere and laminar disk, respectively. It indicates the ratio of the surface area of a sphere with the same volume as the cell to the actual surface area of the cell,

$$Sphericity = 4.84 \frac{V^{2/3}}{SA} \tag{3.2}$$

Since erythrocytes are required to be flexible enough to squeeze through small capillaries and it is known that a small increase in the area of a membrane results in hemolysis [13], the "non-sphericity" of red blood cells is essential to their ability to deform. The mean sphericity index calculated for all 1,537 cells is 0.72.

Minimum Cylindrical Diameter (MCD): The MCD is a theoretical geometric parameter that indicates the thinnest cylindrical channel that a given erythrocyte could squeeze through. The MCD for an erythrocyte population is based on the idea that the most efficient shape for a cell to pass through a narrow capillary is similar to that of a hot dog [9]. The MCD is related to the volume and surface area as

$$V = SA * MCD - \frac{\pi MCD^3}{12} \tag{3.3}$$

Calculating the smallest cylinder an erythrocyte can pass through is relevant since aged or diseased cells are removed from the blood stream though a filtering system which depends on geometric constriction.

The distributions shown for sphericity and MCD differ significantly from those reported by Canham and Burton [9]. These differences are expected and unavoidable due to differences in the measurement techniques, especially sample preparation. It is clear that the cells measured by DPC are, on average, both smaller in diameter and thinner. This difference could be due to either difference in sample preparation or a bias towards thicker, rounder cells in the measurements of Canham and Burton.

The relationship between cell volume, surface area and shape determines the cells' ability to deform and thus successfully deliver oxygen by squeezing through capillaries much smaller than their diameter. From the distributions alone it is difficult to determine the nature of these geometric constrictions and it is therefore necessary to study the correlations between the

parameters measured [3]. The plots of volume vs. diameter, surface area vs. diameter and surface area vs. volume are shown in Figure 3.3. The plots indicate a linear relationship rather than higher power law dependence as previously shown by Canham and Burton. It is also evident from these geometric constrictions and from the description of cellular shape by the sphericity index that cells with larger volumes should tend to be thinner than those with smaller volumes. The fact that there is an upper limit on the sphericity as the cell volume increases is illustrated in Figure 3.3d. Furthermore, from the constant MCD lines superimposed on the surface area vs. volume plot in Figure 3.3c, it can be seen that Equation (3.3) predicts the linear boundary that limits the distribution.

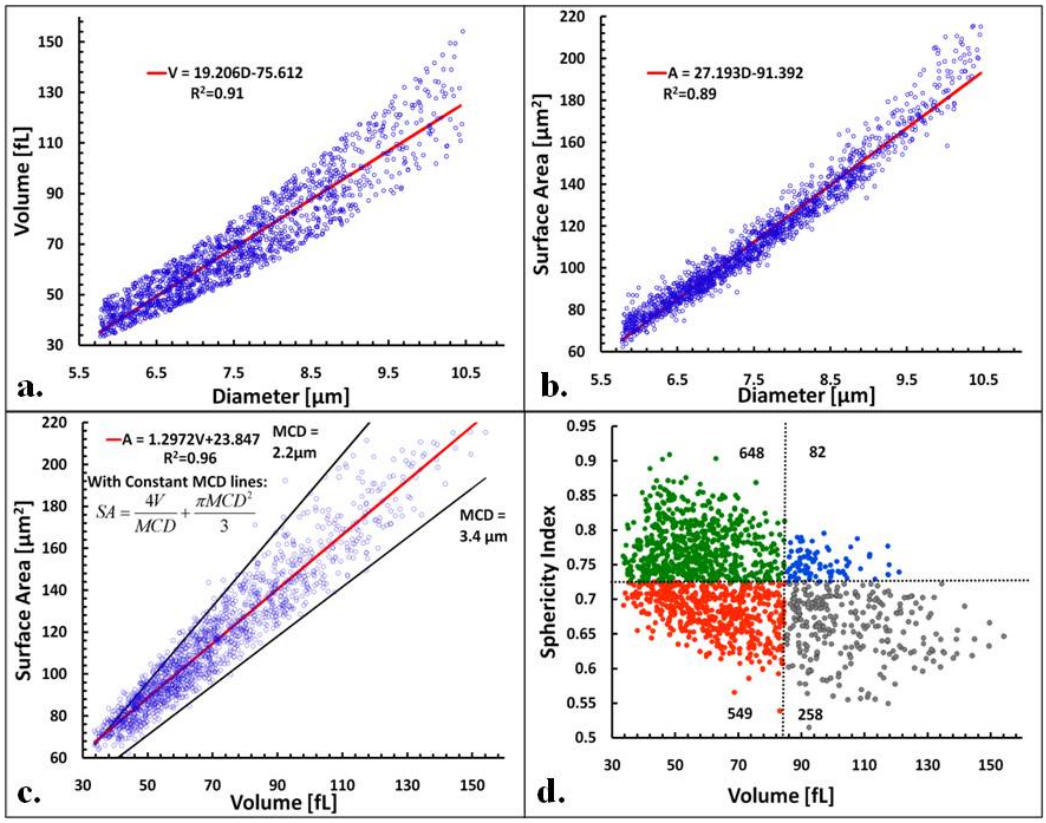

Fig. 3.3 Red lines are linear fits with R^2 values shown in the legend. a) Volume vs. diameter, b) surface area vs. diameter, c) surface area vs. volume with constant MCD lines shown in black, d) sphericity index vs. volume, quartered to show that cells with larger volume are thinner.

It is remarkable that despite the differences in the histograms of the individual parameters between our measurements and those of Canham and Burton, the relationships between the measured parameters are very close. The deviations that exist are reasonable based on the differences between test subjects; this is supported by the differences in the data between the subjects tested by Canham and Burton. Since the accuracy of our technique is supported based on the 4.5 μm microspheres measured and since the previously defined relationships between RBC geometrical parameters hold true, the dissimilarities between our measurements and those reported in the literature could be attributed to all the reasons discussed above, including measurement techniques, sample preparation and physiological conditions of test subjects.

3.4 Conclusions

In summary, we have presented a novel adaptation of diffraction phase microscopy by utilizing a commercial compact disk as a diffraction grating in the sample plane. A dynamic spatial filtering system was implemented using spatial light modulation via a commercial liquid crystal projector, which allowed us to attenuate the object field in order to achieve maximum fringe contrast. We demonstrated the ability of the DPC system to take cytometry measurements of human erythrocytes and calculated several parameters. Out of these parameters, i.e. volume, surface area, sphericity and minimum cylindrical diameter, only the first is commonly available from most hematological measurement methods such as flow cytometry and centrifugation. We show that the correlations between the measured volume, surface area and diameter display the same linear relationships that have been reported previously, including the geometric constriction on the data predicted by the minimum cylindrical diameter model.

In the future we plan to make this technique more feasible as an inexpensive “lab-on-a-chip” type medical instrument by integrating DPC with existing CD-ROM drive technology. A CD-

ROM based method of medical diagnosis would make this technology immediately available to the over 1 billion people who have access to modern computers and would allow for quick and easy diagnosis of a large variety of physiological conditions.

4. CLINICAL APPLICATIONS

4.1 Moving to the Clinic

We employed Diffraction Phase Cytometry (DPC), which is designed to produce accurate measurements of normal blood and in addition is capable of characterizing specific morphological abnormalities in diseased blood. The simplicity and versatility of the DPC technique was demonstrated in the last section by combining it with CD-ROM technology for characterizing red blood cells (RBCs) [14]. By giving access to detailed 2D and 3D morphological parameters such as volume, surface area, sphericity, diameter, etc., DPC provides new information that is currently unavailable from commercial instruments. It is known that the distributions of these parameters and correlations between them reveal physiologically important information about a given blood sample [9]. For example, the minimum cylindrical diameter (MCD) can be used to predict the minimum capillary diameter that a given cell can squeeze through [15].

We present a comparison between the abilities of the DPC system and a state-of-the-art clinical impedance counter to measure and characterize RBCs. It is shown that after taking the mean cell hemoglobin concentration (MCHC) into account the DPC data correlates very well with the impedance counter. The advantages of using the DPC are also illustrated by an analysis of the volume and sphericity distributions obtained from two patients. DPC also has the advantage that it can be easily implemented as an add-on modality to a microscope without adding any additional preparatory steps to the lab workflow. The results shown here are from measurements on whole blood samples, further illustrating the flexibility of the technology, as it can be applied to both perpherial blood smears or to samples stored according to clinical protocols. Considering the agreement with current techniques and the detailed morphological

information provided by the DPC, it could prove to be both a powerful diagnostic tool and a way to improve blood testing efficiency by reducing the number of cases that require a manual smear analysis.

4.2 Materials and Methods

Whole blood is drawn from patients at a local community hospital via venepuncture by a certified phlebotamist and is stored in EDTA coated containers at room temperature. A complete blood count (CBC) analysis is then performed on each sample with the Coulter LH50 (Beckman-Coulter) impedance counter used for routine analysis in the hematology lab at the hospital. Each sample is marked with a unique identifier, and all unique personal patient information (name, id#, etc.) is removed in compliance with HIPPA regulations and the University of Illinois Institutional Review Board to maintain patient confidentiality.

The whole blood is then diluted with the same Coulter LH series diluent (Beckman Coulter) used by the impedance counter for a final concentration of 0.2% whole blood in solution. This concentration was chosen as it provides an adequate cell count for comparison with the CBC while being low enough to provide sufficient distribution of the cells, which is necessary for proper analysis given the large variations in patient hematocrit. Following dilution, the sample is pipetted into a 200 μm tall chamber, which is made in house by punching a hole in double-sided Scotch tape (3M) and sticking one side of the tape to a cover slip. After the sample is introduced to the chamber, it is sealed using another cover slip. This sealed chamber technique reduces the mechanical stress imposed on the cells during sample preparation, offers precise control over the sample volume, prevents drying, and reduces cell translation. The samples are measured 5 minutes after being sealed to allow them to settle to the bottom of the chamber and to reach a steady state in the solution.

The DPC setup utilized in this experiment uses the diffraction phase microscope [3, 16] as its core platform. In short, the DPC setup is a common path interferometer, in which a diffraction grating located at the image plane of a microscope is used to generate diffraction orders, each containing full spatial and phase information of the sample. The 0^{th} order or un-deviated beam is then spatially low-pass filtered using a pinhole in the Fourier plane so that it can be used as a reference beam; the +1 diffraction order is used as the sample beam and all the other orders are blocked. A second lens is then introduced to project the interferogram onto the CCD plane for recording. The phase map of the sample is then retrieved from a single CCD exposure by applying a spatial Hilbert transform [17].

For each sample, 1600, 32 μm x 32 μm interferograms are recorded, which cover a total area of 1.64 mm^2; a total of 5.3 minutes is required to scan this area at a rate of 5 frames/s. The analysis of the phase images is carried out in MATLAB (The Mathworks 2008) using a cell detection and analysis software developed in house. To find the cells in each image a standard particle detection algorithm is used [12]. Once the pixels occupied by individual cells are identified we can proceed to quantify the 2D and 3D morphological parameters of each cell. The 2D parameters such as diameter, projected area and circularity are easily obtained using region property descriptors available in MATLAB.

In order to obtain physiologically relevant and accurate 3D parameters from the retrieved phase map we translate it to a height map using an index of refraction calculated based on the mean cell hemoglobin concentration of each sample, as measured by the impedance analyzer. Due to the linear dependence on the protein concentration [18], the refractive index can be calculated as $n_c = n_0 + \beta * MCHC$, where β is the refractive increment of hemoglobin (0.002 dL/g) and MCHC is the concentration of dry protein expressed in g/dL. The phase map φ(x,y) is

then translated to a height map h(x,y) using the contrast in refractive index between the cells and surrounding media, Δn: $h(x,y) = \frac{\lambda}{2\pi\Delta n}\phi(x,y)$, where λ =532 nm is the wavelength of the illumination and $\Delta n = n_c - n_0$. Once the height information is retrieved, the volume of each cell is calculated by integrating the height map over the projected area as $V = \iint h(x,y)dxdy$. The surface area of individual cells is determined using Monge parameterization [19], where the area of each pixel element, dA, is calculated as $dA = dxdy\sqrt{1 + h_x^2 + h_y^2}$ where dx and dy are the width and height of each pixel and h_x and h_y are the gradients along the x and y directions respectively. The surface area of each cell is then the sum of all the area elements and the projected area, assuming the cell is sitting flat on the cover slip. Knowing the surface area and volume, we can calculate parameters such as sphericity (ψ) and minimum cylindrical diameter (MCD). The sphericity, ψ, of RBCs was first determined as an important parameter by Canham and Burton [9]. It is defined as the ratio between the surface area (SA) of a sphere with the same volume as the cell, to the actual surface area of the cell, with values ranging from 0 (for a laminar disk) to 1 for a perfect sphere, and is calculated as $\psi = 4.84\frac{V^{2/3}}{SA}$. The MCD, also introduced by Canham and Burton, is a theoretical parameter that predicts the smallest capillary diameter that a given RBC can squeeze through. The MCD is obtained by solving the following polynomial equation that defines the cell volume: $V = SA * MCD - \frac{\pi MCD^3}{12}$.

Overall, for each cell imaged we obtain the following 17 parameters: *perimeter, projected area, circular diameter, surface area, volume, sphericity, eccentricity, minimum, maximum and mean height, minimum cylindrical diameter, circularity, integrated density, kurtosis, skewness*

and variance. Thus, it is possible to identify and characterize abnormal cells that would otherwise be difficult or impossible to detect manually in a smear. This type of analysis could be utilized for early detection of diseases, infections and abnormalities such as poikliocytosis [5] and malarial infection [20], or of reactions to treatments such as chemotherapy and bone marrow transplants [21]. If manual analysis of the abnormality is still necessary to confirm the diagnosis, a physician may simply examine the cell images that have been labeled as abnormal by the DPC system, rather than manually scanning a smear in search of abnormalities. Given the wealth of information available about each cell, it is possible to study the distributions of and correlations between parameters in order to establish the parameters expected from a normal sample and to characterize various abnormalities.

4.3 Comparative Study

In this study, samples from 32 patients were analyzed using both a clinical Coulter impedance counter and the DPC system; with the DPC system we analyzed an average of 828 cells per sample. We show that there is high correlation between the CBC and DPC data and provide examples of the advantages associated with our interferometric, image-based cytometry technique.

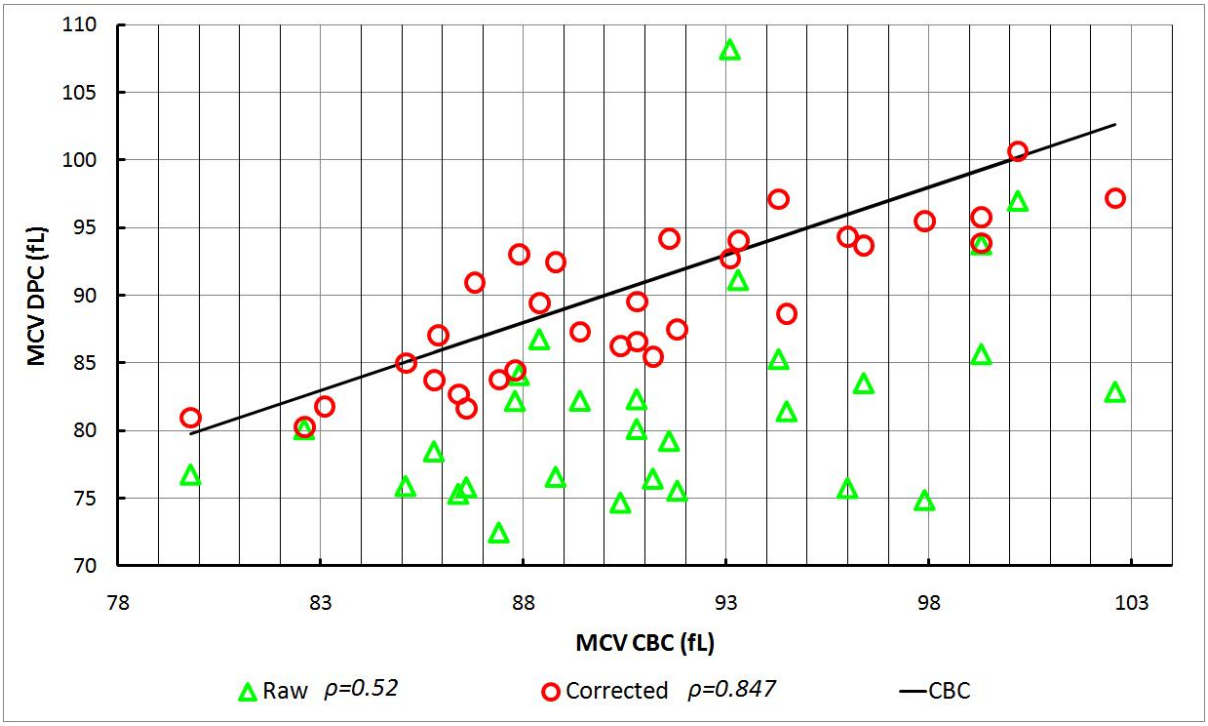

Fig. 4.1 MCV values measured by DPC vs. impedance counter (complete blood count, CBC). The DPC data is shown before the correction for the refractive index (Raw) and after refractive index correction (Corrected). Pearson correlation coefficients for both data sets are shown in the legend. The straight line, included for comparison, represents the CBC MCV values.

In order to evaluate the consistency of the DPC analysis in comparison to that of the Coulter counter, we compared the mean corpuscular volumes (MCV) obtained by both methods (Fig. 1). Initially the data was analyzed assuming a constant refractive index contrast for all samples, which resulted in a weak correlation (Pearson correlation coefficient, ρ=0.52) between the DPC and CBC volume data (circular symbols in Figure 4.1). However, once the MCHC values are taken into account and the refractive index contrast is corrected, the correlation improves to ρ=0.84 (triangular symbols in Figure 4.1).

The MCHC is currently used by pathologists to help diagnose abnormalities such as anisochromasia (large variation in MCHC) and spherocytosis (high MCHC) [6]. However, with current automated counters a pathologist has to manually examine a smear to confirm diagnosis of spherocytosis or any other morphological abnormalities which would result in an abnormal

MCHC distribution. With the current DPC system it is possible to provide this diagnosis directly using the spherecity index. Figure 4.2 is an example of a sphericity distribution obtained from a 97-year-old female patient exhibiting anisocytosis (diagnosed by a large variation in MCV). By examining cell images along the sphericity distribution, the capabilities of the DPC to differentiate between flat and spherical cells is made clear. If a larger spherocytic subpopulation were to exist in this patient, it would appear as a secondary maximum in the distribution or could be identified by a positive shift in the samples mean sphericity value.

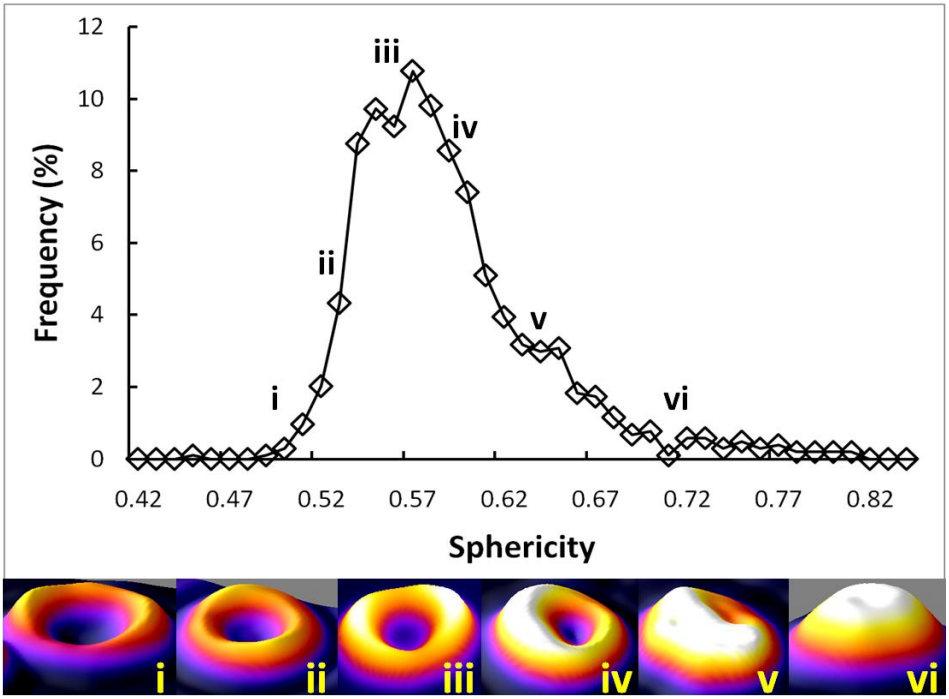

Fig. 4.2 Comparison of cells across the sphericity distribution for a 97 y/o female patient exhibiting anisocytosis. Examples of cells at the sphericity values as follows: i) 0.50 ii) 0.54 iii) 0.57 iv) 0.61 v) 0.65 vi) 0.72.

An important advantage of DPC as an emerging technology is that it recovers all metrics that are familiar and intuitive to pathologists, such as the MCV. One disorder that is fairly common and easy to diagnose using the MCV is anisocytosis, which is characterized by large variations in the cell volumes and quantified by the red cell distribution width (RDW). Figure 4.3 shows volume distributions from two patients, one normal and one exhibiting anisocytosis.

Again we show images of cells across the distribution to illustrate the information available about each cell.

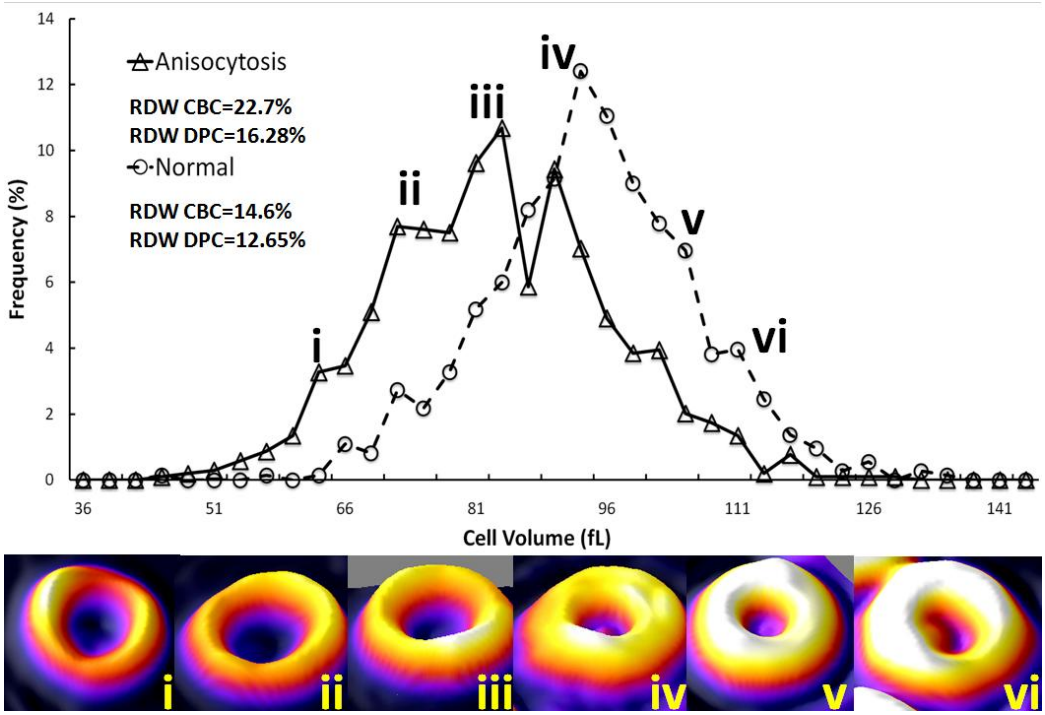

Fig. 4.3 Comparison of volume distributions of patient exhibiting anisocytosis vs. a normal patient. The DPC measures red cell distribution width (RDW) values of 12.65 and 16.28 for the normal and abnormal patient respectively. More subpopulations are apparent in the patient with anisocytosis. Examples of cells at the different volume peaks as follows: i) 64 fL ii) 72 fL iii) 84 fL iv) 93 fL v) 102 fL vi) 117 fL.

This type of analysis enables the DPC system to accurately identify the morphological abnormalities that are responsible for the anisocytosis. Since anisocytosis could be a result of a variety of disorders such as thalassemia (decreased globin synthesis) and myelodisplastic syndrome (preleukimia) [6], more detailed information on the cause will aid in a quick and early automatic diagnosis of these conditions.

4.4 Conclusions

We have demonstrated the ability of the DPC system to operate as an automatic blood analyzer, which recovers the parameters provided by current clinical instruments. We showed that the additional set of parameters measured by DPC offers insight into the nature of the

numerical abnormalities used to identify morphological disorders. Using this type of analysis may aid in an automatic diagnosis of conditions that currently require manual smear analysis. Even though the current DPC system has lower throughput and speed than state-of-the-art impedance counters, these are practical issues which can be overcome due to the rapid advances in automated image acquisition and processing technologies.

The strong dependence of our results on the cell hemoglobin content indicates that an accurate measurement of individual cell protein content needs to be made. A previous method entails measuring the cells in two solutions with different refractive indices [22]. Though this decoupling method is an effective way to calculate the refractive index, it may be impractical in a clinical setting, due to throughput considerations and because exposing the cells to different solutions may affect their properties. It has recently been shown that DPC can directly measure single cell hemoglobin concentration by either utilizing a broadband source [23] or performing DPM at different wavelengths [24]. Both of these techniques rely on the dispersion properties of hemoglobin to infer the protein concentration. These new methods free the DPC from relying on any external measurements and thus greatly add to both is practical application in a clinic and its power in aiding differential diagnosis.

In conclusion, DPC offers a powerful new blood screening utility that can be used to aid in making differential diagnosis by an experienced pathologist. DPC can be simply added on as a modality to any existing microscopy, and no special sample preparation is necessary to integrate it into the clinical workflow. Furthermore, the outputs of DPC are intuitive morphological characteristics, such as sphericity and skewness, meaning that no new specialized knowledge is necessary to take advantage of DPC. Advancements in spectroscopic phase measurements,

image processing and computing power will continue to augment the abilities of DPC, while maintaining its position as a low cost, high throughput and highly sensitive instrument.

5. DISCUSSION

Currently we can accurately and reliably measure phase in three spatial dimensions and time which provides access to a great amount of information. However, as the blood screening experiments showed, we are missing an important dimension in our phase measurements: the wavelength dependence. Part of my future work will thus be focused on gaining access to this fifth dimension. This may be accomplished by either using multiple sources of wavelengths or by getting wavelength dependent phase information in a white light setup. The first goal with this will be to measure the hemoglobin concentration at the single cell level. The phase that is measured is a function of wavelength:

$$\Delta\phi(\mathbf{r};t,\lambda) = \frac{2\pi\Delta n(\mathbf{r};t,\lambda)}{\lambda} h(\mathbf{r},t) \tag{5.1}$$

The refractive index may be written as

$$\Delta n(\mathbf{r};t,\lambda) = \beta(\lambda) C_{Hb}(\mathbf{r};t) + n_{H2O}(\lambda) - n_s(\lambda) \tag{5.2}$$

Here C_{Hb} is the concentration of hemoglobin. From measurements at two wavelengths this may be calculated as

$$\frac{\Delta\phi(\mathbf{r};t,\lambda_1)}{\Delta\phi(\mathbf{r};t,\lambda_2)} = \frac{\lambda_2\Delta n(\mathbf{r};t,\lambda_1)}{\lambda_1\Delta n(\mathbf{r};t,\lambda_2)} \tag{5.3}$$

$$C_{Hb}(\mathbf{r};t) = \frac{\lambda_2\Delta\phi(\mathbf{r};t,\lambda_2)\left[n_{H2O}(\lambda_1) - n_s(\lambda_1)\right] - \lambda_1\Delta\phi(\mathbf{r};t,\lambda_1)\left[n_{H2O}(\lambda_2) - n_s(\lambda_2)\right]}{\beta_1\lambda_1\Delta\phi(\mathbf{r};t,\lambda_1) - \beta_2\lambda_2\Delta\phi(\mathbf{r};t,\lambda_2)} \tag{5.4}$$

Measuring the hemoglobin concentration will enable DPC to provide comprehensive blood screening and may also open up new diagnostic opportunities based on the spatio-temporal behavior of the hemoglobin concentration. This idea may then be extended to provide chemical specificity in more complex systems. In conclusion, the results shown above further establish that

QPI techniques have great potential to address relevant clinical needs and answer important biological questions.

REFERENCES

[1] F. Zernike, "How I discovered phase contrast," *Science,* vol. 121, no. 3141, pp. 345-349, Mar. 1955.

[2] E. Abbe, "Beitrage zur theorie des mikroskops und der mikroskopischen wahrnehmung," *Arch. Mikrosk. Anat.,* vol. 9, no. 1, pp. 413-418, Dec. 1873.

[3] G. Popescu, T. Ikeda, R. R. Dasari and M. S. Feld, "Diffraction phase microscopy for quantifying cell structure and dynamics," *Opt. Lett.,* vol. 31, pp. 775-777, Mar. 2006.

[4] M. Piagnerelli *et al.*, "Assessment of erythrocyte shape by flow cytometry techniques," *J. Clin. Pathol.,* vol. 60, pp. 549-554, Jun. 2007.

[5] B. J. Bain, *Blood Cells: A Practical Guide*, 3rd ed., Oxford: Blackwell Science, 2002.

[6] B. J. Bain, "Diagnosis from the blood smear," *N. Engl. J. Med,* vol. 353, no. 5, pp. 489-507, Aug. 2005.

[7] D. J. Stephens and V. J. Allan, "Light microscopy techniques for live cell imaging," *Science,* vol. 300, pp. 82-86, no. 4, Apr. 2003.

[8] Z. Wang, L. J. Millet, M. U. Gillette and G. Popescu, "Jones phase microscopy of transparent and anisotropic samples," *Opt. Lett.,* vol. 33, no. 7, pp. 1270-1272, Dec. 2008.

[9] P. B. Canham and A. C. Burton, "Distribution of size and shape in populations of normal human red cells," *Circ. Res.,* vol. 22, pp. 405-422, Mar. 1968.

[10] Y. L. Jin, J. Y. Chen, L. Xu and P. N. Wang, "Refractive index measurement for biomaterial samples by total internal reflection," *Phys. Med. Biol.,* vol. 51, no. 20, pp. 371-379, Oct. 2006.

[11] M. Hammer, D. Schweitzer, B. Michel, E. Thamm and A. Kolb, "Single scattering by red blood cells," *Appl. Opt.,* vol. 37, no. 31, pp. 7410-7418, Nov. 1998.

[12] R. C. Gonzalez, R. E. Woods, and S. L. Eddins, *Digital Image Processing Using MATLAB*, Upper Saddle River, NJ: Prentice-Hall, 2003.

[13] R. P. Rand and A. C. Burton, "Area and volume changes in hemolysis of single erythrocytes," *J. Cell. Comp. Physiol.,* vol. 61, no. 3, pp. 245-253, Mar. 1963.

[14] M. Mir, Z. Wang, K. Tangella and G. Popescu, "Diffraction phase cytometry: Blood on a CD-ROM," *Opt. Exp.,* vol. 17, no. 4, pp. 2579-2585, Feb. 2009.

[15] P. B. Canham, "Difference in geometry of young and old human erythrocytes explained by a filtering mechanism," *Circ. Res.,* vol. 25, pp. 39-45, May 1969.

[16] H. Ding, Z. Wang, F. Nguyen, S. A. Boppart and G. Popescu, "Fourier transform light scattering of inhomogeneous and dynamic structures," *Phys. Rev. Lett.,* vol. 101, no. 23, p. 238102, Dec. 2008.

[17] T. Ikeda, G. Popescu, R. R. Dasari and M. S. Feld, "Hilbert phase microscopy for investigating fast dynamics in transparent systems," *Opt. Lett.,* vol. 30, no. 10, pp. 1165-1167, May 2005.

[18] G. Popescu *et al.*, "Optical imaging of cell mass and growth dynamics," *Am. J. Physiol. Cell. Physiol.,* vol. 295, pp. C538–C544, Jun. 2008.

[19] S. A. Safran, *Statistical Thermodynamics of Surfaces, Interfaces, and Membranes*: Reading, MA: Addison-Wesley, 1994.

[20] Y. K. Park *et al.*, "Refractive index maps and membrane dynamics of human red blood cells parasitized by *Plasmodium falciparum*," *Proc. Natl. Acad. Sci.,* vol. 105, no. 37, pp. 13730-13735, Sep. 2008.

[21] G. d'Onofrio *et al.*, "Simultaneous measurement of reticulocyte and red blood cell indices in healthy subjects and patients with microcytic and macrocytic anemia," *Blood,* vol. 85, no. 3, pp. 818-823, Feb. 1995.
[22] B. Rappaz *et al.*, "Comparative study of muman erythrocytes by digital holographic microscopy, confocal microscopy, and impedance volume analyzer," *Cyto. A,* vol. 73A, pp. 895-903, May 2008.
[23] H. Ding and G. Popescu, "Instantaneous spatial light interference microscopy," *Opt. Exp.,* vol. 18, no. 2, pp. 1569-1575, Jan. 2010.
[24] Y. K. Park, T. Yamauchi, W. Choi, R. Dasari, M. S. Feld, "Spectroscopic phase microscopy for quantifying hemoglobin concentrations in intact red blood cells," *Opt. Lett.,* vol. 34, no. 23, pp. 3668-3670, Dec. 2009.